Chapter 6

Phase transitions in Liquid crystals under negative pressures

6.1   Introduction

In the previous chapter we have described the effect of compression i.e. positive pressure on liquid crystals. We also reported that in room temperature liquid crystal samples mounted in the high pressure (HP) cell if the *volume is fixed* an excess pressure gets generated at high temperatures. In an analogous manner, if a given volume of liquid is cooled from high temperatures, a negative pressure can be generated in the medium. In this chapter we describe the *first* experiments on the effect of tensile stress on liquid crystals.

Condensed matter can sustain *negative pressures* because of attractive interactions between molecules. Under negative pressures the intermolecular distance *r* increases, and the medium which is under tension is in a *metastable* state [1]. Indeed at a sufficiently high *negative* pressure, the medium goes over to the equilibrium high density state by *cavitation* [1]. Several natural phenomena crucially depend on such a state: for example, sap-ascent in tall trees [2] and the initial inflationary phase in the expansion of the universe [3]. The latter is analogous to the cavitation phenomenon which occurs in a liquid under tension, usually due to thermal fluctuations. Maris and Balibar [4] have shown that quantum fluctuations induce cavitation in the superfluid phase of Helium-4. Ice I has a lower density than water, and the phase transition between them has been studied under negative pressures [5]. Liquid crystals exhibit several phase transitions involving changes in appropriate symmetries [6,7] and are ideally suited for investigating such transitions between phases in *both* of which the medium is under tension. To achieve large negative pressures small drops have to be cooled under constant volume (i.e. isochoric) conditions. We have developed a technique of subjecting liquid crystals to negative pressures by embedding small droplets (of diameter ∼ 100 μm) of mesogens in a matrix of a glass-forming material. We have carried out the *first* measurements of birefringence $\Delta\mu$, a measure of orientational order parameter *S*, on such samples. An isochoric cooling of the sample is used to locate transitions under negative pressures, from the isotropic to nematic as

well as from nematic to smectic A phases. We present the temperature variations of Freedericks threshold voltage [7] V_{th} which is a measure of a curvature elastic constant for both isochoric as well as isobaric conditions.

The structures adopted by soft condensed materials depend on a balance between repulsive and attractive interactions. Onsager [8] demonstrated in a seminal paper over half a century ago that colloidal suspensions of hard rods can undergo a transition from the isotropic to the nematic phase due to packing effects alone, as the density is increased. The anisotropic attractive interactions are quite important for rod-like organic molecules of low molecular weight and the nematic to isotropic (NI) transition occurs at relatively high densities.

It is known that the NI transition is of first order nature [7]. The Landau –de Gennes (LdG) theory describes the NI transition quite well (see section 1.6). The free energy density is given by

$$F_{LdG} = \frac{a}{2}(T - T^*)S^2 - \frac{B}{3}S^3 + \frac{C}{4}S^4 \qquad\qquad 6.1$$

where the third order term with coefficient B is nonzero in view of the second rank tensor nature of the orientational order parameter S. This term leads to a first order NI transition in which the orientational order parameter S jumps from zero to a finite value (usually ~ 0.3) at T_{NI}. T^* is a hypothetical second order transition point which is slightly below T_{NI}. Experiments show that the density ρ also jumps by ~0.2% at T_{NI}, clearly indicating that the order parameter is coupled to density. The LdG model has been extended by Mukherjee and co-workers [9] to incorporate density –order parameter coupling, by assuming the relevant term to be $S^2\partial\rho^2$. The term $\partial\rho = \rho_N - \rho_I$ is the difference in density between nematic and isotropic phases. But this term would not discriminate between the positive and negative signs of $\partial\rho$, which is inappropriate. We have extended the LdG model by adding the appropriate coupling terms. By comparing the isobaric as well as isochoric measurements of $\Delta\mu$ we have estimated the coefficients coupling S and density ρ of an extended LdG model of the nematic phase.

Experimentally T_{NI} - T^* is about 1 to 2 ^{0}C, while the molecular mean field theory of Maier and Saupe would give a much larger value [6,7]. Indeed it has been shown by Tao et al [10] that the inclusion of a density dependent intermolecular interaction can reduce this discrepancy. The relative importance of density and temperature in determining the variation of order parameter has been investigated by measurements of both the order parameter and the density as functions of pressure above 1 bar in a couple of cases [11]. Experiments under constant volume (ie., isochoric) conditions are ideally suited for such an investigation. As the temperature is lowered, such a medium will have a density which is *lower* than in equilibrium and hence it will be in a <u>metastable</u> state. The medium experiences a tensile stress, i.e., *negative* pressure, which increases in magnitude as the temperature is lowered. The medium can go over to the stable state by cavitation, i.e., by developing a vapour bubble, which grows to the required size if at nucleation it has a radius r beyond a critical value r^*. A vapour embryo of radius r has an energy $E_r = -\dfrac{4}{3}\pi r^3 P + 4\pi r^2 \sigma$ where P is the magnitude of the negative pressure and σ the surface tension. E_r has a maximum with a potential barrier height of $16\pi\sigma^3/3P^2$ at $r^* = 2\sigma/P$.
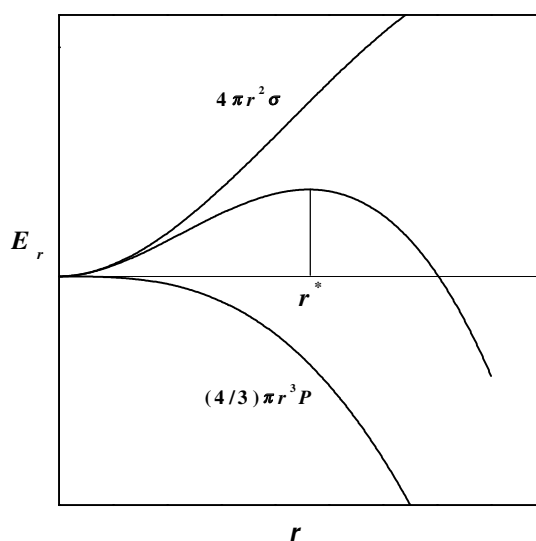

Figure 6.1: A schematic representation of the energy E_r of a vapour bubble as a function of the radius r.

A schematic representation of the energy of a vapour bubble as a function of its radius r is shown in Figure 6.1. The barrier height is *lowered* at larger negative

pressures. Extraneous influences like surface non-uniformities can lower the barrier considerably and lead to heterogenous nucleation of bubbles.

A technique for creating very large negative pressures (~ -1kbar) by isochoric cooling of small water drops embedded in quartz crystals was developed some years ago by Zheng et al [12]. It has been used to approach the homogeneous nucleation limit for cavitation [12], which corresponds to a first order transition from the (low density) metastable to the (normal density) stable state of the medium.

It would be of obvious interest to extend such studies to liquid crystals and other soft materials to explore their properties under tensile stress under which the effect of attractive interactions is relatively enhanced. Organic compounds cannot withstand high temperatures used to encapsulate water droplets. Several techniques have been developed during the past couple of decades for embedding relatively small ($\sim$ a few μm) spherical liquid crystal droplets in polymer matrices [13]. The polymer dispersed liquid crystals (PDLCs) exhibit very interesting electro-optic responses and have been used in commercial display devices which do not require polarisers. The liquid crystals partially dissolve in the polymer matrix. In view of the visco-elasticity of the polymer and the small size of nematic drops, cavitation phenomena have not been noticed in PDLCs.

Our strategy to overcome the above problems was to embed the liquid crystal drops in a matrix made of a glass-forming material. The glass transition point T_g has to be moderately high, but not above 200 ^{0}C to prevent thermal decomposition of the liquid crystal molecules. Another requirement is that the liquid crystal compounds should not dissolve in the glass forming material.

6.2   Experimental

6.21   Preparation of sample

After testing a few different materials, we found sucrose, a carbohydrate to be suitable for embedding liquid crystalline drops. The melting point of sucrose $T_m \simeq 180$ ^{0}C   and the glass transition temperature, $T_g \simeq 78$ ^{0}C [14]. As it is a carbohydrate, it does not dissolve in most of the mesogenic compounds whose

molecules have phenyl rings. Spherical drops are not suited for measurements of optical anisotropy of the liquid crystal. In order to be able to apply an electric field to the sample, we prepare it between ITO (Indium tin oxide) coated glass plates. The ITO plates were coated with a thin layer of polyimide, cured and subsequently unidirectionally rubbed using a soft tissue. This ensures that the nematic director aligns along the rubbing direction. One of the plates is kept on an aluminium block which is heated to about 185 ^{0}C. A small quantity of sucrose mixed with some glass spacers of thickness ~ 10 μm is placed on the glass plate. Liquid crystal is added when the sucrose melts and starts to flow. The second ITO plate is placed on the melt such that the rubbing directions of the two plates are parallel to each other allowing for homogeneous alignment of the liquid crystal molecules. The top plate is pressed against the bottom one, and the sandwich is suddenly cooled to room temperature. Care is taken to ensure that the sandwiched sample is present only in the center of the cell leaving an air gap all around. The thickness of the sample t is estimated by measuring the thickness of the air gap present in the cell using an Ocean Optics interference spectrometer (see section 1.7). Cells with uniform thickness are chosen for the optical path difference measurement. A typical sandwich of sucrose with embedded liquid crystalline drops is shown in Figure 6.2. Note that all the liquid crystal drops are aligned homogeneously indicating that the liquid crystal molecules touch the confining glass plates and are confined in the glassy matrix of sucrose.
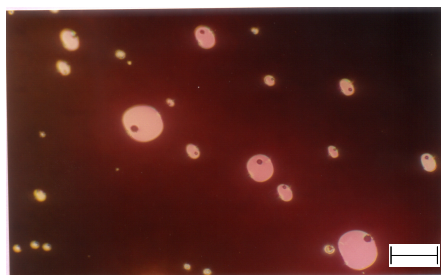

Figure 6.2: Photomicrograph of aligned nematic drops of CBCC embedded in a glass matrix of sucrose, between crossed polarisers set at 45^0 to the rubbing direction. Note the cavities in all the drops. Scale bar corresponds to 270 μm.

6.22 Optical phase difference measurement

As the size of liquid crystal droplets is of a few 100μm, the transmitted intensity measurement method used for estimating birefringence of thick samples discussed in previous chapters is not suitable for measurement of absolute phase difference as there will be an effect due to the surrounding glassy sucrose which is *optically* isotropic. So to measure the absolute path difference we have used a quarter wave plate in conjunction with the polarisers.
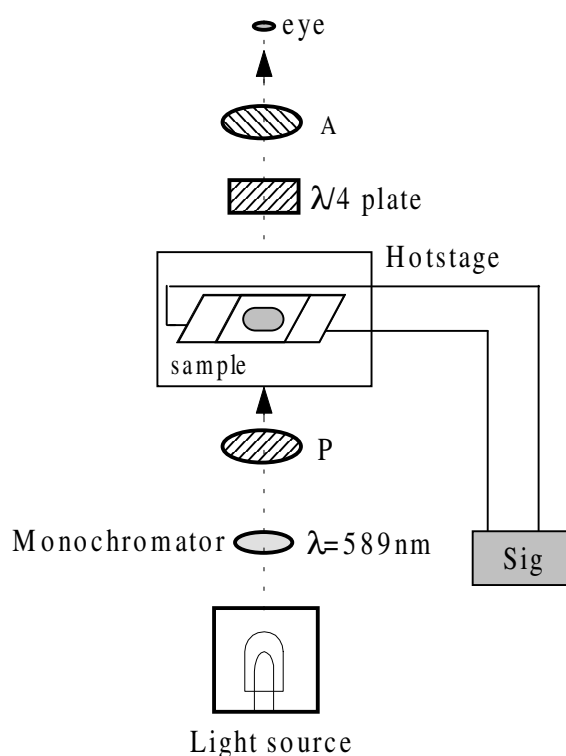

Figure 6.3: Schematic diagram of experimental setup used to measure the optical phase difference of sample. Sig: Signal generator, P: Polariser, A: Analyser.

The schematic diagram of the experimental setup used in the optical phase difference measurement is shown in Figure 6.3. The sample is mounted in a hot-stage (Instec HS1) which is controlled using a temperature controller (Instec MK2) to an accuracy of 5 mK. The hot-stage is mounted on the rotating stage of a polarising microscope (Leitz Orthoplan) between crossed polarisers. A large liquid crystal drop with a diameter ~ 100 μm and having good orientation of the sample in the liquid crystalline phase is chosen for measurements. The measurements were carried out by visually observing the sample at the center of the chosen drop to avoid edge effects.

The optical phase difference measurements were carried out using the quarter wave plate compensation technique described in section 4.23. As mentioned in chapter 4, when the polarised light beam passes through a birefringent liquid crystal whose principal axes are at 45^0 to the electric vector of the light beam, the emergent beam consists of two linearly polarised components of equal amplitudes, one component being phase shifted by $2\pi t\Delta\mu/\lambda$ with respect to the other, where λ is the wavelength of incident beam and t the sample thickness. When these two orthogonal components pass through a quarter wave plate arranged as described in section 4.2 (Figure 6.3), they are converted into two circularly polarized beams of opposite sense. Superposition of these beams yields a linearly polarised light beam with its direction of vibration rotated by $\pi t\Delta\mu/\lambda$ with respect to the direction of vibration of the light beam incident on the liquid crystal. The analyser is rotated by an angle ϑ to get the dark field of view. This angle ϑ is a measure of the optical phase difference $\Delta\phi$ and is given by $\vartheta = \pi t\Delta\mu/\lambda$. The measurements were made at temperature steps of 40mK between T_{NI} and $T_{NI} -3 \, ^0C$ as the variation of $\Delta\mu$ is quite steep in that range. At lower temperatures the measurements are carried out at temperature steps of $0.1 \, ^OC$ or larger steps depending on the rate of the variation of $\Delta\mu$ with temperature. The absolute value of optical phase difference $\Delta\phi$ $(=2\pi t\Delta\mu/\lambda)$ is determined using Freedericks transition technique (see section 1.25, chapter 1). The voltage for Freedericks transition experiment was applied using a signal generator (Sig: Wavetek model 395) at a frequency of 2.1KHz. We have also measured the Freedericks threshold voltage V_{th} as a function of temperature. The temperature variation of $\Delta\mu$ is calculated using the measured values of ϑ.

The liquid crystal systems used in the study are (i) p-cyanophenyl carboxylate (CBCC) with the phase transition sequence: crystal 54.8 ^0C - N - 68.3 ^0C - I, (ii) a mixture (MCB) of 30 wt% of 4-octyl-4′-cyanobiphenyl (8CB) with 4-octyloxy 4′ - cyanobiphenyl (8OCB) with the phase transition sequence: SmA_d - 57.8 ^0C - N -70 ^0C - I (iii) mixtures of 8OCB with 4-hexyloxy 4′ -cyanobiphenyl (6OCB) which exhibits N-SmA_d-N_r phase sequence in a narrow range of concentration of 6OCB. All the compounds were obtained from Messrs Roche. The chemical structures of compounds along with their transition temperatures are given in Figure 6.4.
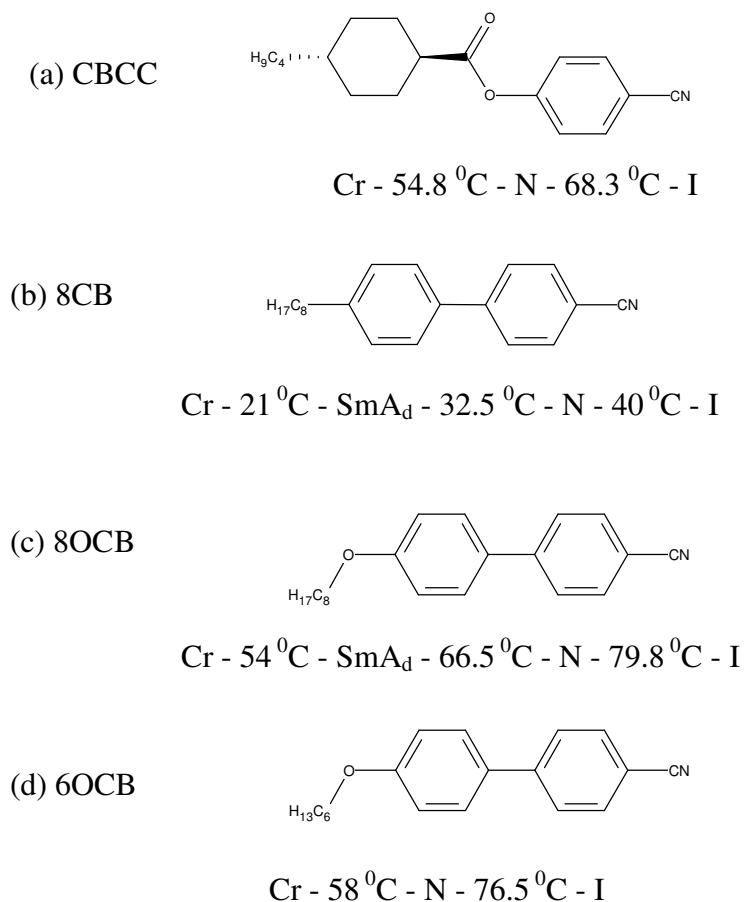
(a) CBCC

Cr - 54.8 ^{0}C - N - 68.3 ^{0}C - I

(b) 8CB

Cr - 21 ^{0}C - SmA$_d$ - 32.5 ^{0}C - N - 40 ^{0}C - I

(c) 8OCB

Cr - 54 ^{0}C - SmA$_d$ - 66.5 ^{0}C - N - 79.8 ^{0}C - I

(d) 6OCB

Cr - 58 ^{0}C - N - 76.5 ^{0}C - I

Figure 6.4: Chemical structures of compounds used in the experiments and their transition temperatures.

6.3   Results and Discussion

6.31 Estimation of birefringence   under isochoric and isobaric conditions

(i)   CBCC

On isochoric (constant volume) cooling of the liquid crystal drops embedded in the sucrose glass matrix the negative pressure steadily increases and finally at a sufficiently high *negative* pressure the low density *metastable* liquid crystal goes over to the higher density stable liquid crystal by spontaneous *cavitation* (formation of vapour bubble). Indeed in a given sample all the liquid crystal droplets cavitate practically at the same temperature   indicating that the cavity is nucleated homogeneously (Figure 6.2). On heating a sample of CBCC with cavity to temperatures well above the isotropic phase the cavity vanishes around 74 ^{0}C. The isochoric measurement of optical phase difference is then carried out on cooling the

sample from the isotropic phase. The nematic phase supercools below the melting point and cavitation occurs around 35 ^{0}C. The optical phase difference measurements are continued down to room temperature. The photograph of a nematic drop of CBCC embedded in glassy sucrose matrix before the formation of cavity and after formation of cavity are shown in Figure 6.5.
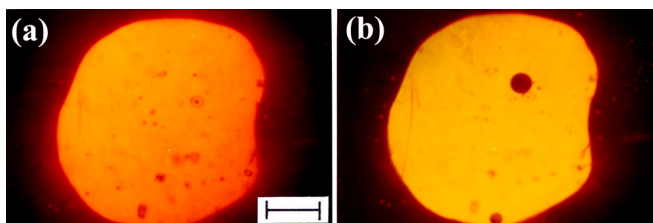

Figure 6.5: Photograph of a large drop of CBCC embedded in a glass matrix of sucrose between crossed polarisers set at 45^0 to the rubbing direction. The scale bar corresponds to 160 μm. (a) appearance of the drop before the formation of cavity and (b) after cavitation.
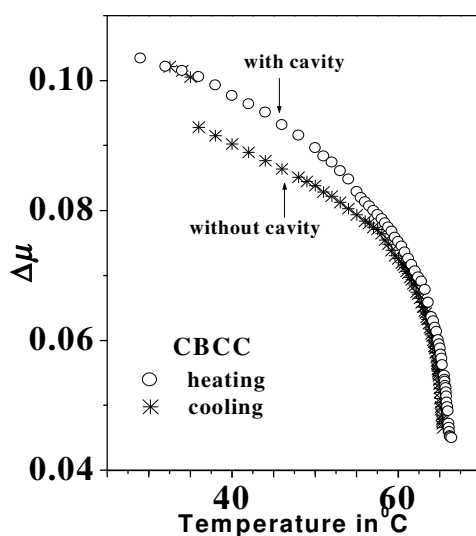

Figure 6.6: Temperature dependence of the birefringence Δμ, measured in the nematic phase of an embedded drop of CBCC. A jump in Δμ can be noticed after the formation of cavity in the cooling mode.

The measurements of optical phase difference are then made in the heating mode, right upto the NI transition point. The temperature variations of Δμ of samples both in the absence of cavity i.e., isochoric measurement, as well as in the presence of cavity (essentially isobaric condition) are calculated using the measured value of ϑ.

The results are shown in Figure 6.6. It may be noted from Figure 6.6 that at any temperature, $\Delta\mu$ is *lower* for the drop without a cavity, i.e., in the *metastable* nematic under negative pressure, compared to that for the drop with the cavity, in which the density is higher. The increase in $\Delta\mu$ with decreasing temperature under isochoric condition i.e. sample without cavity is due to the variation of *temperature alone*. It may be noted that there is a sudden increase in $\Delta\mu$ of ~ 7% in a first order phase transition at cavitation. The variation of $\Delta\mu$ in the sample with cavity is associated with variations of both temperature and density. Independent $\Delta\mu$ measurements were also made on CBCC at atmospheric pressure using a sample taken between two ITO coated glass plates, without sucrose matrix. These values compare well with the data obtained for the drops with cavity as shown in Figure 6.7. Further the data agree with the measurements of Takahashi et al [15] (see Figure 6.7).
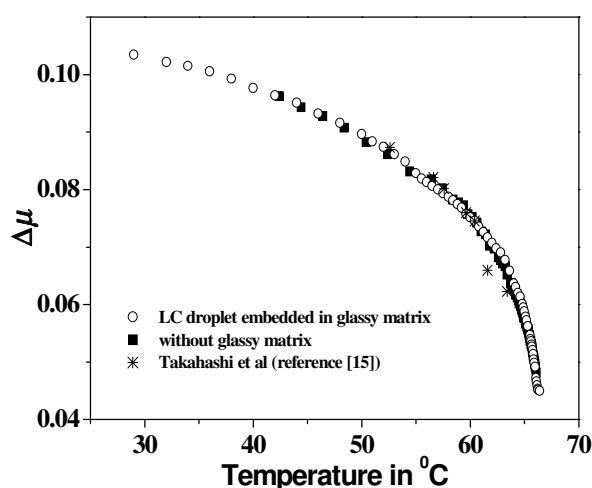

Figure 6.7: The temperature variations of birefringence $\Delta\mu$ of CBCC measured using a sample with cavity for a liquid crystal drop embedded in glassy matrix and a sample taken between ITO coated plates (without sucrose matrix) at atmospheric pressure. The data from Takahashi et al [15] are also shown for comparison.

The orientational order parameter $S \approx \Delta\mu/\Delta\mu_0$, where $\Delta\mu_0$ is the value of birefringence in the fully aligned state. The isochoric order parameter is significantly smaller than the isobaric value, the difference between the two increasing at lower temperatures (Figure 6.6). CBCC has a cyclohexane ring (Figure 6.4a), and thus has a

smaller value of $\Delta\mu$ compared to a nematogen with two phenyl rings. For the drops without cavity T_{NI} is 0.9 ^{0}C lower than that in the presence of cavity. Using the dP/dT_{NI} value of CBCC (chapter 5), the *negative* pressure is estimated to be ~ 22 bars at T_{NI}.

(ii)   MCB

A photograph of aligned drop of MCB embedded in glass matrix of sucrose is shown in Figure 6.8. On heating a sample of MCB with cavity to temperatures well above the isotropic phase the cavity vanishes around ~76 ^{0}C.
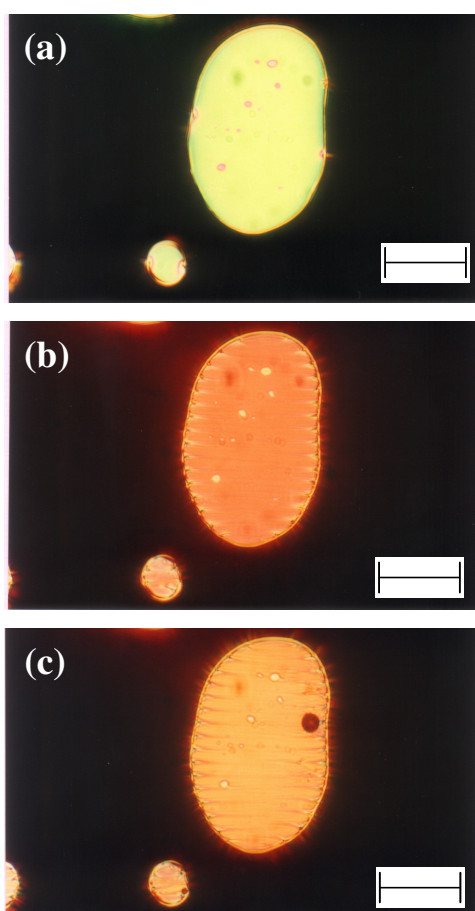

Figure 6.8: Photomicrographs of an aligned drop of MCB (a) in the nematic phase at 63 ^{0}C, (b) in the smectic phase (note the focal conic defects at the boundary) at 53 ^{0}C before the formation of cavity and (c) in the smectic phase at 40 ^{0}C after cavitation. Note that the cavitation has occurred in both the large and small drops. (Scale bar corresponds to 70 μm.)

The measurements were carried out on this sample using the procedure described above for CBCC. The temperature variations of $\Delta\mu$ of the samples both in the absence of cavity i.e. isochoric measurement, as well as in the presence of cavity (essentially isobaric condition) are shown in Figure 6.9. In MCB the cavitation occurs at 40 ^{0}C in the SmA$_d$ phase and the value of $\Delta\mu$ suddenly increases by ~6% at the first order transition.
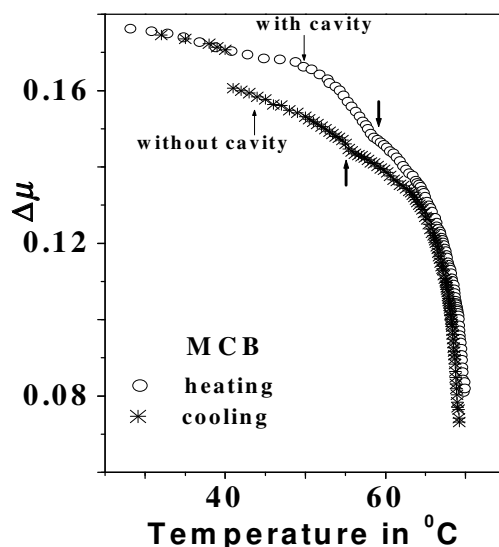

Figure 6.9: Temperature dependence of the birefringence $\Delta\mu$, measured in the nematic as well as smectic phases of an embedded drop of MCB. The thick arrow indicates SmA$_d$-N transition. A jump in $\Delta\mu$ can be noticed after the formation of cavity in the smectic phase in cooling mode.

We have carried out independent measurement of $\Delta\mu$ on a sample taken between two ITO coated glass plates without sucrose matrix. And the result of this matches with the temperature variation of $\Delta\mu$ of the sample with cavity (Figure 6.10). In MCB isochorically measured T_{NI} and T_{AN} are lower by 0.6 ^{0}C and 1.8 ^{0}C respectively compared to the measurements in drops with cavity. Using the dP/dT values for MCB reported in chapter 5 the estimated negative pressures are ~25 bars at T_{NI} and ~129 bars at T_{SmAN}. Extrapolating this the cavitation in MCB occurs at a negative pressure of ~ 230 bars. The smallness of magnitude of negative pressure at cavitation compared to that in water is related with the low surface tension which is ~ 25 dynes/cm for 8CB [16] compared to ~ 80 dynes/cm for water.
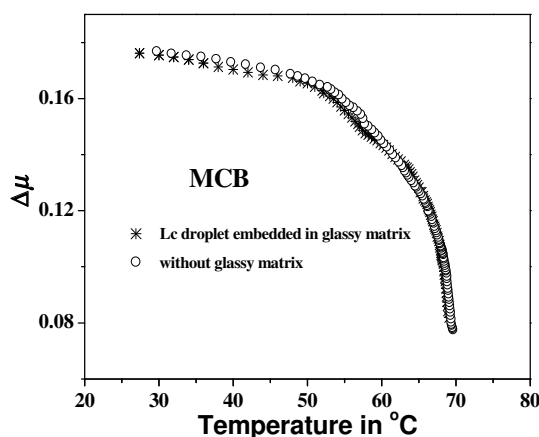
Figure 6.10: The temperature variations of birefringence $\Delta\mu$ of MCB measured using a sample with cavity for a liquid crystal drop embedded in glassy matrix and a sample taken between ITO coated plates (without sucrose matrix) at atmospheric pressure.

6.32 An extended Landau de Gennes theory to take into account density- order parameter coupling

As mentioned in section 4.42, the limitation of LdG theory is that it is a mean field theory valid near the NI transition point. Hence we use the data points within $\sim 1^0$ below T_{NI} for analysis.

The density jumps at the NI transition indicating that the order parameter S is coupled to density (see section 6.1).We write the density dependent terms of the free energy as

$$F_\rho = -\frac{M}{2}\partial\rho S^2 + \frac{\Lambda}{2}\partial\rho^2 \qquad 6.2$$

in which the first term ensures that the density increases with increase in order parameter, which has a positive sign for rod like molecules for better packing. The second term is the energy cost of changing the density from its equilibrium value in the isotropic liquid.

At a *fixed pressure*, the density adjusts itself to minimize F_ρ, yielding

$$\partial\rho = \frac{MS^2}{2\Lambda}$$ 6.3

The total free energy is $$F = F_{LdG} + F_\rho$$ 6.4

Substituting for the $\partial\rho$ in the equation for total free energy, we get

$$F = \frac{a}{2}(T-T*)S^2 - \frac{B}{3}S^3 + \frac{C'}{4}S^4$$ 6.5

where $$C' = C - \frac{M^2}{2\Lambda}$$ 6.6

On heating the sample with the cavity, the latter reduces in size and finally disappears at a temperature T_o in the isotropic phase. In the *isochoric* case, the density ρ is fixed and $\partial\rho$ is given by

$$\partial\rho = \rho_o - \rho_{is}(T)$$ 6.7

where ρ_o is the density at temperature T_o, and

$$\rho_{is}(T) = \rho_o\left(1 + \alpha(T_o - T)\right)$$ 6.8

with α being the co-efficient of thermal expansion.

Using this value of $\partial\rho$, and minimising the total free energy (equation 6.4) with respect to S, we get

$$\left(a + M\rho_o\alpha\right)T = aT* + BS - CS^2 + M\rho_o\alpha T_o$$ 6.10

The orientational order parameter $S \approx \Delta\mu/\Delta\mu_0$, but we do not know $\Delta\mu_0$. Using the density data available in the literature for CBCC [15], $\Delta\mu$ values within ~ 1 ^{0}C of T_{NI} in both isobaric and isochoric samples have been least square fitted to the appropriate equations. The density data on 8CB and 8OCB are reported by Karat et al and Sen et al respectively [17]. Using these values, the density of the mixture MCB at any relative temperature (T_{NI}-T) is estimated as an appropriate average over the mole fractions of 8CB and 8OCB [17]. The results of the fit for both CBCC and MCB are shown in Figure 6.11a and Figure 6.11b respectively. We write $\beta = B/\Delta\mu_0^3$ and $\chi = C'/\Delta\mu_0^4$ and $m = M/\Delta\mu_0^2$. The order parameter at the NI transition point at constant pressure, $S_{NI} = 2B/3C'$ [7] (see section 1.8) can be written as $S_{NI} = 2\beta/(3\chi\Delta\mu_0)$. Also $S_{NI} \approx \Delta\mu_{NI}/\Delta\mu_0$, hence $\Delta\mu_{NI} = 2\beta/3\chi$.

From equation 6.3 $\partial\rho_{NI} = \dfrac{MS_{NI}^2}{2\Lambda}$, which can be rewritten as $\partial\rho_{NI} = \dfrac{m\Delta\mu_{NI}^2}{2\Lambda}$ in terms of $\Delta\mu_{NI}$, the birefringence at the NI transition point. The list of fit parameters is presented in Table 1.
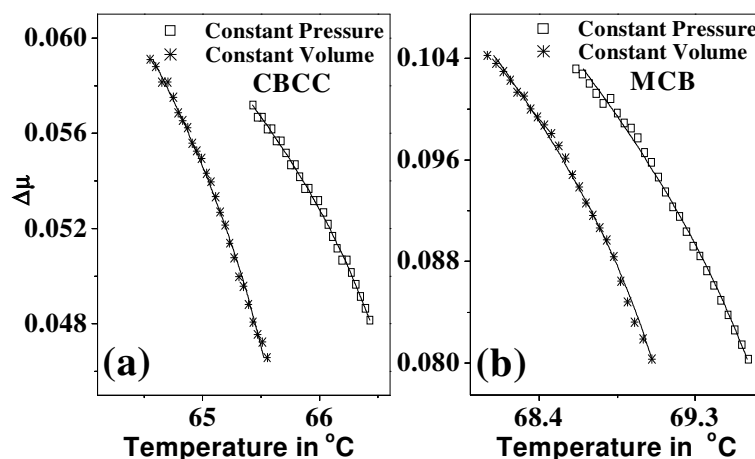

Figure 6.11: The birefringence data within about 1^0 of T_{NI} in both constant pressure and constant volume conditions fitted to the phenomenological model described in the text for (a) CBCC and (b) MCB.

CBCC	MCB
T_{NI} = 339.5K T^*=338 K $\alpha = 8.5\times10^{-4}$ cgs units $a/(\Delta\mu_o)^2 = 3.2\times10^7$ cgs units $B/(\Delta\mu_o)^3 = 1.08\times10^{10}$ cgs units $C/(\Delta\mu_o)^4 = 1.49\times10^{11}$ cgs units $C'/(\Delta\mu_o)^4 = 1.369\times10^{11}$ cgs units $M/(\Delta\mu_o)^2 = 3.8\times10^{10}$ cgs units $\Lambda = 6.1\times10^{10}$ cgs units	T_{NI} = 342.9K T^*=339.9 K $\alpha = 10\times10^{-4}$ cgs units $a/(\Delta\mu_o)^2 = 2.9\times10^7$ cgs units $B/(\Delta\mu_o)^3 = 2.98\times10^9$ cgs units $C/(\Delta\mu_o)^4 = 2.345\times10^{10}$ cgs units $C'/(\Delta\mu_o)^4 = 2.29\times10^{10}$ cgs units $M/(\Delta\mu_o)^2 = 7.0\times10^9$ cgs units $\Lambda = 4\times10^{10}$ cgs units

Table 1: List of parameters corresponding to the least square fit of the data shown in Figure 6.11.

The estimated values of $\Delta\mu_{NI}$ for CBCC and MCB are 0.052 and 0.086 respectively which are higher compared to those observed experimentally (Figure 6.11). The jump in density at the NI transition point $\partial\rho_{NI}$ calculated using these values of $\Delta\mu_{NI}$ are 8.6 ×10^{-4} g/cc and 6.6 ×10^{-4} g/cc for CBCC and MCB respectively. The density data on CBCC reported by Takahashi et al [15] is not accurate near T$_{NI}$. From Vuk's model $\dfrac{\overline{\mu^2}-1}{\overline{\mu^2}+2}=\dfrac{4\pi}{3}\dfrac{N_A\rho\overline{\alpha}}{M}$, where $\overline{\mu}^2=\left(\mu_e^2+2\mu_o^2\right)/3$, N_A is the Avogadro number, ρ the density, M the molecular weight, $\overline{\alpha}$ is the average polarizability. Using the reported value of $\overline{\alpha}$ and the measured values of μ_e and μ_o [15] the density ρ as a function of temperature is estimated. The value of $\partial\rho_{NI}$ (at constant pressure) estimated using the above method is = 20×10^{-4} g/cc. This value of $\partial\rho_{NI}$ is larger compared to that estimated using the theoretical fit. Using an appropriate average mole fractions of 8CB and 8OCB the value of $\partial\rho_{NI}$ for the mixture MCB is estimated and is =18×10^{-4} g/cc. Again this value is larger compared to that got from the theoretical fit. The discrepancy in the estimated values of $\Delta\mu_{NI}$ and $\partial\rho_{NI}$ using LdG theory compared to those measured experimentally shows the inadequacy of the theory even near the transition point. It may be noted that for both CBCC and MCB the value of Λ reported in Table 1 is of the order of inverse compressibility for typical mesogens [6].

6.33 Freedericks transition experiments

As a consequence of the apolar nature of nematic director $\hat{n}$ an external electric field $\vec{E}$ couples to the medium through its dielectric anisotropy $\Delta\varepsilon$ and the orientational part of the dielectric energy density is given by $-\varepsilon_0\Delta\varepsilon\,(\hat{n}\,.\,\vec{E}\,)^2/2$, where ε_0 is the vacuum dielectric constant. If $\hat{n}$ is strongly anchored at the two glass plates (which is the usual case), $\hat{n}$ reorients in the center of the cell at a threshold voltage $V_{th}=\pi\sqrt{K_{11}/\varepsilon_0\Delta\varepsilon}$ (independent of the sample thickness t) where K_{11} is the splay elastic constant relevant to the initial distortion of the director [7]. In the highly polar compounds the dielectric anisotropy $\Delta\varepsilon$ mainly depends on the dipolar contribution.

According to Maier and Meier's theory the expression for the dielectric anisotropy is given by

$$\Delta\varepsilon = (\varepsilon_{\parallel} - \varepsilon_{\perp}) = 4\pi \frac{N_A \rho \ hF}{M}\left[\Delta\alpha - F\left(\frac{p^2}{2k_BT}\right)(1 - 3\cos^2\beta)\right]S$$

where $\Delta\alpha(=\alpha_l - \alpha_t)$, is the anisotropy of polarizability of a perfectly oriented medium, N_A is the Avogadro number, ρ the density, M the molecular weight, $h = 3\bar{\varepsilon}/(2\bar{\varepsilon}+1)$, is the cavity field factor and $F = 1/(1 - f \ \bar{\alpha})$ where $f = (\bar{\varepsilon}-1)/[2\pi a^3 (2\bar{\varepsilon}+1)]$ is the reaction field factor for spherical cavity and $\bar{\alpha}$, is the average polarizability, p is the molecular dipole moment. Hence for cyano compounds, $\Delta\varepsilon$ is $\propto \rho S/T$. In the mean field approximation [7], K_{11} is proportional to S^2. As such $V_{th}^2/T \propto S$. Indeed, as shown in Figure 6.12, for both the systems the value of V_{th}^2 is higher for the nematic sample with the cavity compared to that without cavity.
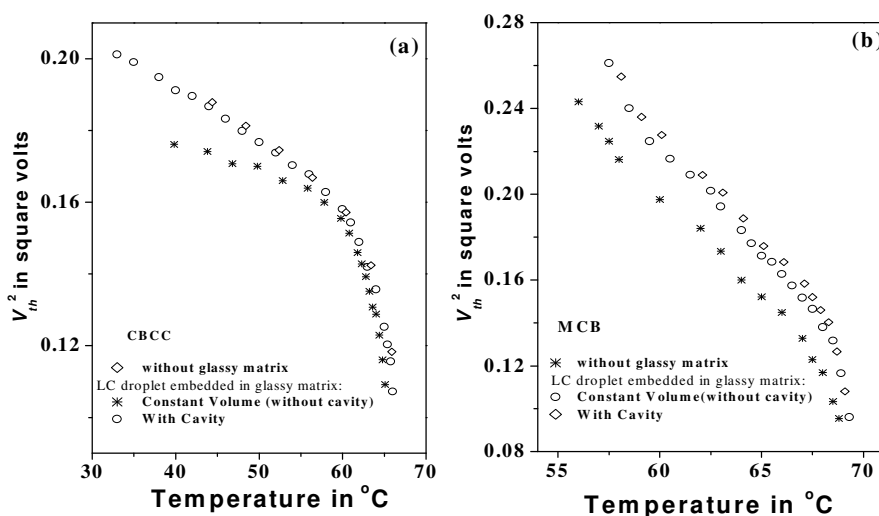

Figure 6.12: Temperature variations of the square of the threshold voltage for splay distortion of the nematic phase of (a) CBCC and (b) MCB.

Again, V_{th}^2 values measured in ordinary cells at atmospheric pressure for both the systems compare well with the values obtained for the drops with cavities (Figure 6.12). In CBCC, which exhibits only the nematic phase $V_{th}^2/T \propto S$. The proportionality constant $V_{th}^2/T\Delta\mu \approx 0.0063$ (to within $\pm 1.5\%$) for the drops both with and without cavity. In MCB, smectic like short-range order grows as the SmA-N

transition is approached. As such the mean field theory is no longer valid and $V_{th}^2/T\Delta\mu$ varies from 0.003 to 0.0055 for the drop both with and without cavity as the temperature is lowered.

6.34 Phase diagram of a binary mixture exhibiting reentrant nematic transition

The binary mixtures of 6OCB and 8OCB exhibit N-SmA$_d$-N$_r$ phase sequence in a narrow range of concentrations of 6OCB (see Figure 5.6). We have constructed the P-T phase diagram for a mixture with 27.5 mol% of 6OCB, and as expected, the SmA$_d$ phase gets suppressed beyond ~75bars as shown in Figure 5.7. The value of P_m, the maximum pressure up to which the SmA$_d$ phase is stable decreases with increasing concentration of 6OCB [18]. The concentration-temperature phase diagram of the mixtures studied in droplets embedded in a sucrose glass matrix is shown in Figure 6.13. The transition temperatures of samples with cavity, which were measured while heating the samples, match with those measured at atmospheric pressure on samples without the sucrose matrix.
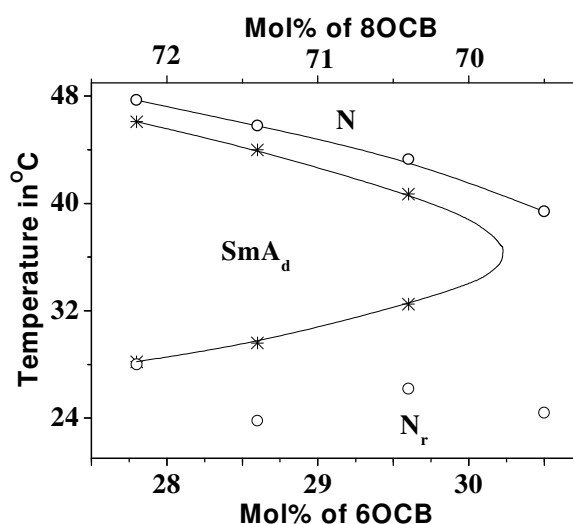

Figure 6.13: The concentration-temperature phase diagram of binary mixtures of 6OCB with 8OCB. ✳ corresponds to samples with cavity (isobaric condition). The N-SmA$_d$ transition points of isochorically cooled samples fall on a smooth curve (upper circles). The lower circles represent the cavitation temperatures, at which transition from SmA$_d$ phase under tension to N$_r$ phase at normal pressure takes place.

On *isochoric* cooling of the samples, the thermal range of SmA_d widens. In all the samples cooled isochorically, the N-SmA_d transition temperature is higher than that at atmospheric pressure, and the cavitation occurs in the SmA_d phase. With the sudden increase in density, the sample immediately goes over to the reentrant nematic phase. Thus the lower circles in Figure 6.13 represent the cavitation temperatures rather than the SmA_d-N_r transition temperatures under isochoric condition. The latter would have occurred at much lower temperatures, but are preempted by the cavitation. In the mixture with 27.8 mol% of 6OCB, the cavitation occurs at a temperature close to the SmA_d-N_r transition point of the sample with cavity. Thus negative pressures *expand* the thermal range of SmA_d phase substantially. The sample with 30.5 mol% of 6OCB does not exhibit the SmA_d phase at atmospheric pressure. This phase is <u>induced</u> on isochoric cooling of the medium. The SmA_d phase of course disappears once the cavitation occurs in the embedded drop (Figure 6.13).

6.4 Conclusions

We have shown that using a simple technique of embedding liquid crystal drops in a glassy matrix of sucrose, the liquid crystals can be subjected to *negative* pressures. We have made the *first* measurements of birefringence, a measure of orientational order parameter S of nematic and smectic liquid crystals under *isochoric* condition. The data should be compared with the predictions of molecular theories which take into account both the hard-rod and attractive intermolecular interactions. For this purpose, it would be better to choose compounds without flexible end chains or the highly polar cyano groups in which the dipolar interactions lead to strong short range order effects. Such materials will have $T_{NI} \sim 100\ ^0C$, and it would be very useful if suitable glass forming materials with $T_g \sim 200\ ^0C$ are identified. Indeed, the technique developed in this work is suitable for many other studies.

References

1. P.G. Debenedetti, *Metastable Liquids*, Princeton University Press, Princeton, 1996.

2. N.M. Holbrook, M.J. Burns and C.B. Field, "Negative xylem pressures in plants: a test of the balancing pressure technique", *Science* **270,** 1193-1194, 1995.

3. A.H. Guth, *The inflationary universe*, Addision-Wesley Publishing Co., Reading, 1997.

4. H. Maris and S. Balibar, "Negative pressures and cavitation in liquid helium", *Physics Today* **53,** 29-34, 2000.

5. S.J. Henderson and R. J. Speedy, "Melting temperature of ice at positive and negative pressures", *J.Phys.Chem* **91,** 3069-3072, 1987.

6. S. Chandrasekhar, *Liquid Crystals*, Cambridge University Press, Cambridge, 1992.

7. P.G. de Gennes and J. Prost, *The physics of liquid crystals*, Clarendon press, Oxford, 1993.

8. L. Onsager, "The effect of shape on the interaction of colloidal particles", *Ann. NY Acad. Sci* **51,** 627-659, 1949.

9. P.K. Mukherjee, T.R. Bose, D. Ghose and M. Saha, "Inclusion of density variation in the Landau-de Gennes theory of the nematic-isotropic phase transition", *Phys. Rev. E* **51**, 4570-4573, 1995.

10. R. Tao, P. Sheng and Z.F. Lin, "Nematic- Isotropic phase transition: An extended mean field theory", *Phys. Rev. Lett.* **70**, 1271-1274, 1993.

11. R. G. Horn and T.E. Faber, "Molecular alignment in nematic liquid crystals: a comparison between the results of experiments at high pressure and predictions based on mean field theories", *Proc.R.Soc.Lond.* **A368,** 199-223, 1979.

12. Q. Zheng, D.J. Durben, G.H. Wolf and C.A. Angell, "Liquids at large negative pressures: water at the homogeneous nucleation limit", *Science* **254,** 829-832, 1991.

13. P.S. Drzaic, *Liquid crystal dispersions*, World Scientific, Singapore, 1995.

14. S.L. Shamblin, X. Tang., L. Chang, B.C. Hancock and M.J. Pikal, "Characterization of the time scales of molecular motion in pharmaceutically important glasses", *J. Phys. Chem.* **B103,** 4113-4121, 1999.

15. M. Takahashi, S. Mita and S. Kondo, "Study on Molecular Polarizabilities of Cyclohexane Derivatives", *Mol. Cryst. Liq. Cryst*. **132**, 53-64, 1986.

16. V. A. Korjenevsky and M.G. Tomilin, "Experimental investigation of the surface energy of a nematic liquid crystal", *Liq. Cryst.* **15,** 643-649, 1993.

17. P.P. Karat and N.V. Madhusudana, "Elastic and Optical Properties of some 4′-n-Alkyl-4-cyanobiphenyls", *Mol. Cryst. Liq. Cryst.* **36**, 51-64, 1976. (for 8CB); S.Sen, P. Brahma, S.K. Roy, D.K. Mukherjee and S.B. Roy, "Birefringence and Order Parameter of Some Alkyl and Alkoxycyanobiphenyl Liquid Crystals", *Mol. Cryst. Liq. Cryst*. **100**, 327-340, 1983 (for 8OCB). (The density of MCB is estimated as an appropriate average, using the mole fractions of 8CB and 8OCB).

18. P. E. Cladis, D. Guillon, F. R. Bouchet and P. L. Finn, "Reentrant nematic transitions in cyano- octyloxybiphenyl (8OCB)", *Phys. Rev. A*. **23**, 2594-2601, 1981.